

## The Coherent Limitation of the Specular X-ray and Neutron Reflectivity on the Characterization of the Physical Vapor Deposition Thin Films

Chih-Hao Lee,<sup>1,2,3,\*</sup> Pei-Yu Chuang,<sup>1</sup> Yu-Shou Lin,<sup>1</sup> and Yu-Han Wu<sup>1</sup>

<sup>1</sup>*Department of Engineering and System Science,  
National Tsing Hua University, Hsinchu, Taiwan 30013*

<sup>2</sup>*Institute of Nuclear Engineering and Science,  
National Tsing Hua University, Hsinchu, Taiwan 30013*

<sup>3</sup>*National Synchrotron Radiation Research Center, Hsinchu, Taiwan 30013*

(Received October 31, 2011)

The problem of non-uniformity in film thickness in the measurement of X-ray and neutron reflectivity is studied in this work. This problem becomes severe when the evaporator source is small and the source to substrate distance is very small. The non-uniformity of the film thickness which exceeds the beam coherent length on the film surface, contributes an additional amount of smearing out the reflectivity data resulting in an inaccuracy in determining the film density and interface roughness. Narrowing down the incident slit size will alleviate this problem with the sacrifice of the dynamic range of reflectivity measurements. In addition, the non-uniformity of the thin film can also be found in the system of island growth of the thin film when the island size is well beyond the surface coherent length of incidence X-rays. In this case, the incidence X-ray coherent length should be improved to avoid the problem.

PACS numbers: 61.05.C, 61.05.cm, 61.05.fj

### I. INTRODUCTION

Specular reflection for both X-rays and neutrons is now a well-established technique for investigating the structure of thin films and interfaces. The intensity of the reflected ray carries information about the depth profile of scattering length density in the direction perpendicular to the surface of the medium [1–3]. The scattering length density for the X-ray reflectivity is proportional to the electron density and for the neutron reflectivity is related to the nuclei concentration and magnetic moment. Therefore, the thickness, scattering length density and the surface or interface roughness of a vacuum deposited thin film can be determined. From these parameters, the material behavior of a thin film, such as interdiffusion, compound formation, surface adsorption/desorption, surface segregation and density variation can also be understood. The scientific driving force behind the development X-rays and neutrons reflectivity is the fact that X-rays and neutrons provide a nondestructive probe with a depth-controlled sensitivity. Another virtue of this technique is that the weak interaction of X-rays and neutrons with condensed matter allows one to interpret the experimental data easily in terms of the Fourier transform of correlation functions. The

---

\*Electronic address: [chlee@mx.nthu.edu.tw](mailto:chlee@mx.nthu.edu.tw)

reflectivity curves are as a function of  $q$ , where  $q$  is the scattering wavevector that directly correlated to the incident angle,  $\theta$ , and the wavelength,  $\lambda$ , in term of  $4\pi\sin(\theta)/\lambda$ . Typically, the thin film thickness can be obtained by fitting the periods of Kiessig oscillation fringes of the reflectivity data. The film density can be obtained by fitting the oscillating amplitudes and the critical angle of the reflectivity data. The interface roughness data can be obtained from the oscillating amplitudes and the global intensity drops of reflectivity curves a function of  $q$  [4, 5], because the reflectivity intensity is roughly proportional to the  $q^{-4}\exp(-\sigma^2q_iq_{i+1})$ , where  $\sigma$  is the interface roughness and  $q_i$  and  $q_{i+1}$  are the wavevectors in the consecutive  $i$  and  $i + 1$  layers. Essentially, the roughness gives a lateral statistical average of the profile of scattering length density. Both the roughness and scattering length density changes affect the oscillation amplitude of Kiessig fringes, therefore, the film density, typically obtained by the fringe oscillation amplitudes, is always entangled with the interface roughness, which makes the accuracy of data fitting somewhat ambiguous.

To extract a precise data of thin film parameters from Kiessig oscillation fringes, a few remarks are needed to be taken care. For example, the applicable range for thin film thickness is typically around a few nm up to several hundred nm. If the film thickness is too thick beyond the instrument resolution, then, the oscillating fringes will be smeared out, resulting in a wrong interpretation of interface roughness or film density. On the other hands, if the film thickness is too thin, then, only less than one Kiessig fringe can be measured, resulting a big error in determining the film parameters. This is due to the limitation of the dynamical range of incident beam intensity and the additional contribution of diffuse scattering background (non-specular reflectivity) from the sample itself. Background subtraction is always important in fitting the interface roughness because it affects the slopes of the global intensity drops, especially at high  $q$  part. The resolution of determining the depth profiles,  $\Delta z$ , strongly depends on the highest  $q$  the sample can be measured.  $\Delta z$  is usually proportional to the  $2\pi/q_{\max}$  [6]. Higher incident beam intensity and lower background from diffuse scattering are two most important factors enable the reflective data to go to high  $q$ . Typically, for a X-ray reflectometer at synchrotron radiation beamline, a dynamical range of 8 orders of magnitude and an excellent incidence beam divergence of less than  $0.02^\circ$  can be achieved. The thin film from 2–200 nm with the density contrast of more than 5% usually can be determined precisely, provided the interface and surface roughness are smaller than 1 nm.

Experimentally, more addition attentions should be paid. For example, if a sample exhibits a figure error larger than the incidence beam divergence, either buckling concave up or convex down, a broadening of rocking curve (in transverse direction) can be readily found. In this case, the simple  $2\theta/\theta$  scan (in longitudinal direction) to measure the reflectivity curve is not sufficient. To handle this figure error problem, a set of rocking curve data should be taken and the integrated intensity of each rocking curve is the real specular reflection data for doing data analysis. Background subtraction can also be done at the same time.

Although the experiment is relatively straightforward, the data analysis and interpretation are more complicated. The most common way to analyze specular X-ray and neutron reflectivity data is to guess a model structure, calculate the reflectivity curve and compare with the experimental one. The data analysis has been traditionally carried out by

a non-linear least-squares fitting using Parratt's recursive relation to calculate reflectivity curve [7, 8]. For this simulation method, the thin film is divided into a small number of parallel sublayers, and each of the parameters such as the scattering length density, thickness and interfacial roughness can be varied until a cost function is minimized. However, the method is said to be model-dependent. One cannot guarantee to give a unique solution even with a reasonable fitting result. It is still better to have more knowledge of the sample structure before fitting. The discrepancy between experimental and calculated reflectivity curves is usually due to a model too simplified, or experimentally, the background subtraction of diffuse scattering, systematic misalignment of the sample, the faceted surface of the thin film, and the presence of several local minima during the fitting. In addition, although the general feature of specular reflectivity can be calculated exactly via Fresnel equation on flat interfaces in the specular direction, the simulated reflectivity curve cannot be the exact one in a real experiment since the incident beam is not strictly monochromatic and well-collimated without beam divergence and the detector has a finite acceptance angle. A convolution procedure has to take into account to simulate the real reflectivity data.

Most of programs available such as IMD, LEPTOS, *motofit*, *parrat32*, *Firefx4c*, and *simRX* to fit the reflectivity data are similar to the above approaches [8]. Usually, these programs assume that the film thickness is uniform. In practical, the thin film thickness is not uniform, especially when we deposited the thin film using a tiny evaporation source, such as laser ablation deposition without scanning the laser probe, or e-gun deposition without wobbling the electron gun. To alleviate the non-uniformity problem, people usually increase the source to substrate distance in order to enhance the thin film uniformity by sacrificing the deposition rate. Another source of non-uniform thin film is the island growth during the deposition when the grown island size is larger than the coherent length. To illustrate these questions clearly, we did several simulations to see the reflectivity curves change due to the non-uniformity of the thin film in the following sections.

## II. FUNDAMENTALS AND SIMULATED REFLECTIVITY CURVES

### II-1. Fundamentals of coherence

Coherence is the degree to which electromagnetic radiation maintains a near-constant phase relationship, both temporally and spatially. Two waves are said to be coherent if they have a constant relative phase. The time over which the phase relationship remains nearly constant is called the coherence time. The path length corresponding to the coherence time is called the coherence length. There are two types of coherence, transverse coherence and longitudinal coherence. The transverse coherence is a measure of spatial coherence. The degree of transverse coherence depends on the beam divergence of the incidence beams. The transverse coherent length,  $\xi_{\perp}$ , can be defined by the slit width or effective source size ( $ds$ ) limiting the beam divergence in the experimental setup and the distance from sample to slits or source ( $Rs$ ). Meanwhile, the longitudinal coherence is a measure of temporal coherence and it reveals the dispersion of wavelength in the propagation direction after an optical wave passes through a certain length. Assume the X-ray or neutron waves travelling

through a coherent length and phase difference can be  $180^\circ$  out of phase, such as:

$$\xi_{\perp}(ds/Rs) = \lambda/2, \quad (1)$$

$$\Delta\lambda(\xi_{\parallel}/\lambda) = \lambda/2. \quad (2)$$

In Eq. (1), we assume the beam divergence is roughly equal to  $ds/Rs$ . The transverse coherent length ( $\xi_{\perp}$ ) is determined by its projection to the divergent beam being  $\lambda/2$  path length delay relative to the central beam. In the Eq. (2), we assume each wavelength difference  $\lambda$  due to the finite energy resolution in each period is accumulated after the X-ray or neutron wave travelling through ( $\xi_{\parallel}/\lambda$ ) numbers of periods, where  $\xi_{\parallel}$  is the longitudinal coherent length. If  $\lambda = 0.2$  nm and  $Rs = 1$  m, and the beam divergence is  $10^{-5}$  rad, then the  $\xi_{\perp}$  is about  $1 \mu\text{m}$ . At the same time, if the energy resolution of a monochromator is  $\lambda/\Delta\lambda = 3000$  for  $0.2$  nm X-ray or neutron, then the  $\xi_{\parallel}$  is about  $300$  nm.

For the geometrical configuration of a reflectivity measurement, see Fig. 1, the surface coherent length (or coherently illuminated length),  $\xi_{\text{surface}}$ , can be related to the  $\xi_{\perp}/\sin(\theta)$  and the depth coherent length is roughly proportional to  $\xi_{\parallel}/(2\sin(\theta))$  if the  $\theta$  is small.

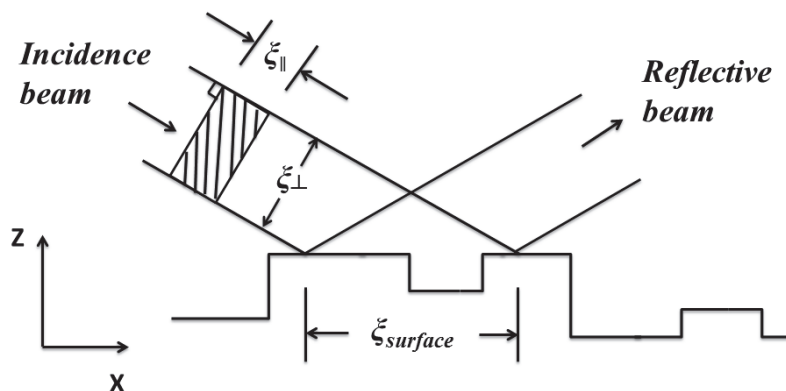


FIG. 1: The surface coherent length on the sample for the X-ray reflected from the surface.

## II-2. Simulated reflectivity curves

This section demonstrates the difference between uniformity and non-uniformity in thickness of a thin film via reflectivity calculation. During the traditional simulation process, it is assumed that the thickness of each layer of a thin film is completely uniform. In this case, we divided the lateral surface into many segments, and in each segment, the thickness of thin film is assumed to be uniform, so that the Parratt formula is valid. The thin film thickness,  $t$ , is assumed to be well within the coherent length of X-ray or neutron so that the interference Kiessig oscillation fringes can be clearly showed when the thin film is uniform. In detail, the conditions of thin film thickness in this study are  $t \ll \xi_{\parallel}/(2\sin(\theta))$ . In this work, a program is written following the Parratt's recursive relation. We did the

simulation calculation by assuming only single deposition layer is present and the resolution of reflectometer is also negligible small. In the island growth or texture calculation beyond the coherent length we assume the top surface is parallel to the substrate surface.

When the thickness of a thin film is not uniform, the path of the incident and reflected waves along the interface might exceed the coherent length. Depending on the coherence length, the simulation can be divided into two cases. The first case is that the coherence length is much larger than the beam illuminated length; while the second one is reversed. There are significant differences in the calculated reflectivity curves based on these two cases even if the thickness is totally uniform. For detail, if we break the footprint of the beam illuminated length on the surface into small pieces of segments with each width of segment well below  $\xi_{\text{surface}}$ . We also assume that the thickness is uniform in each segment, then, the reflectivity intensity,  $R$ , can be calculated as follows.

If the whole footprint length is much larger than  $\xi_{\text{surface}}$ , then

$$R = \left( \sum_i (f_i^* f_i) \right), \quad (3)$$

where  $f_i$  is the scattering amplitude at segment  $i$  and the  $*$  is the complex conjugate. On the other hand, if the footprint is within the  $\xi_{\text{surface}}$ , then the

$$R = \left( \sum_i f_i \right)^* \left( \sum_i f_i \right). \quad (4)$$

The intensity is different calculated by Eq. (3) and Eq. (4).

### III. MODELS OF SPECULAR REFLECTIVITY FOR THE NON-UNIFORMITY THIN FILM

In this study, X-ray reflectivity simulation of a Mo thin film deposited on a soda lime glass substrate was given as an example. This system is important in the fabrication for the system of CuInSe<sub>2</sub> solar cell [9]. The thickness of the Mo thin film is 20 nm at center of the sample, which is well below the depth coherent length of a typical X-ray beam. To simply the calculation, we assumed that the evaporation source is an infinite line source with the diameter much smaller than the source to substrate distance, so that the depositing rate of the Mo atoms on the substrate is inverse proportional to the distance from the evaporation source. The opening width of the detector slit was assumed to be extremely small, so that the detector resolution plays no effect. The sample size was 10 mm and the entrance slit size before the sample was changed from 0.1 mm to 0.4 mm. We also assumed that the intensity of incident beam is uniform across the entrance slit. For the fixed footprint experiment, we assumed the footprint covers exactly on the whole sample size.

To evolve the non-uniformity effect of thin film on the reflectivity data, two different cases are considered here. The first case assumed that the footprint of beam illuminating on the surface is in a fixed area. It can be found in the experiment of neutron time

of flight measurements, X-ray energy dispersive measurements [10, 11], and fixed angle measurements [12–14]. The second case is the traditional  $2\theta/\theta$  scan with fixed wavelength. This is the most common reflectivity measurement in the X-ray community, the sample is moving in  $\theta$  scan and the footprint is roughly proportional to  $1/\sin(\theta)$ .

### III-1. Simulated reflectivity curves with fixed footprint

Fig. 2 shows the reflectivity curve of an e-gun evaporation Mo thin film on a soda lime glass. The distance between the source and substrate,  $D$ , varies from 10 mm to more than 100 mm. The oscillation amplitudes of the Kiessig fringes are damping out at smaller  $D$  due to the non-uniformity of the thin film. At larger  $D$ , the thin film is highly uniform. In fact, the reflectivity curve of  $D = 100$  mm is already very close to the one with  $D = 1000$  mm, which implies the non-uniformity, which can be defined as the maximum difference in thickness across the film, to be within 0.5% is acceptable. In Fig. 3, we show the ratio of peak to valley of the Kiessig fringes around  $q = 0.2 \text{ nm}^{-1}$ ,  $0.3 \text{ nm}^{-1}$ , and  $0.45 \text{ nm}^{-1}$  as a function of  $D$ . The oscillation amplitude of reflectivity curve starts to be smeared out as the  $D$  is smaller than 100 mm. Therefore, for a smaller  $D$ , it is quite possible that the non-uniformity problem leads to a wrong value in roughness or density of the thin film. It should pay additional attention to resolve the actual reason why these oscillation fringes smeared out at high  $q$ . It might come from the increasing roughness, non-uniform thickness or poor instrumental resolution.

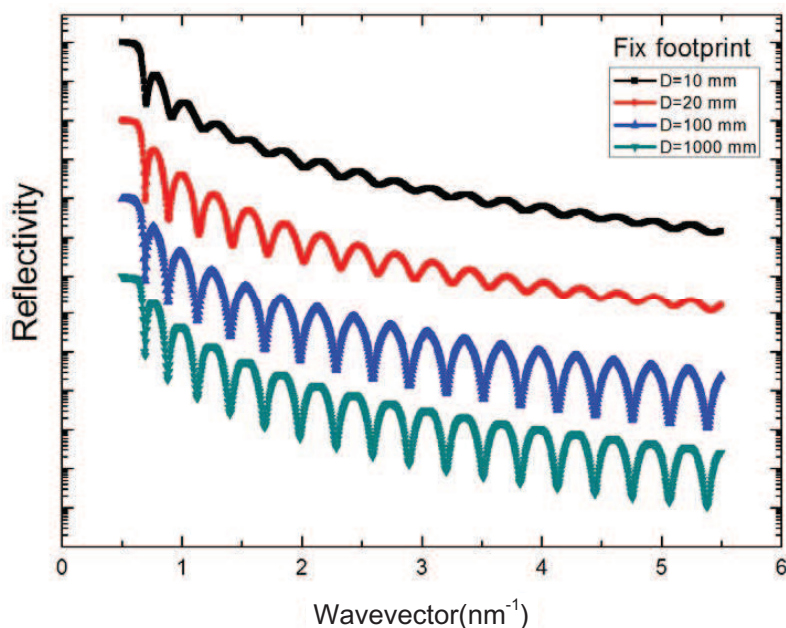


FIG. 2: The reflectivity curves with distances between the source and substrate varying from 10 mm 1000 mm. The X-ray footprints on samples are kept constant.

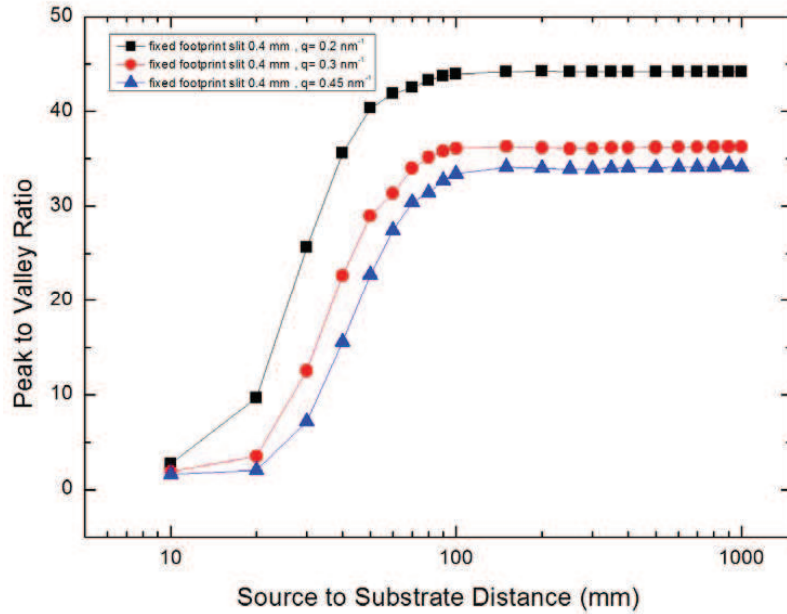


FIG. 3: The ratio of peak to valley of the Kiessig fringes around  $q = 0.2 \text{ nm}^{-1}$ ,  $0.3 \text{ nm}^{-1}$  and  $0.45 \text{ nm}^{-1}$  as a function of the distance between source and substrate. The sample size is 10 mm and the slit size is 0.4 mm.

For the fixed footprint reflectivity experiment, the problem of non-uniform thin film can be reduced by narrowing down the incident slit to give a smaller footprint. In this way, the non-uniformity of the thin film reduced from  $\sim 9\%$  to  $0.5\%$  by closing down the slit from 0.4 mm to 0.1 mm as shown in Fig. 4 for an evaporation system with  $D = 20$  mm.

### III-2. Simulation reflectivity with $2\theta/\theta$ scans

In a typical reflectivity measurement with  $2\theta/\theta$  scan under fixed slit width,  $W$ , the footprint of X-ray illuminated on the sample decreases with incident angle by  $W/\sin(\theta)$ . Thus, the non-uniform problem becomes much alleviated at higher incident angles. For the middle range of  $q$ , the remedy for this non-uniform effect can be done by narrowing down the incident slit. Fig. 5 shows a comparison of the calculated reflectivity curves of the cases between  $2\theta/\theta$  scan and the fixed footprint measurement at  $D = 20$  mm, with all the slits fixed at  $400 \mu\text{m}$ . The calculated result shows that the non-uniformity problem is less severe for the  $2\theta/\theta$  scan than that for the fixed footprint case.

### III-3. The uniformity of island growth thin film

Another kinds of non-uniformity of the thin film is the morphology change during the island growth of the thin film. As the island sizes are much smaller than  $\xi_{\text{surface}}$ , all the heights of islands can be averaged out [15]. When the lateral morphology changes much larger than  $\xi_{\text{surface}}$ , a non-uniformity of the thin film thickness should also be imposed.

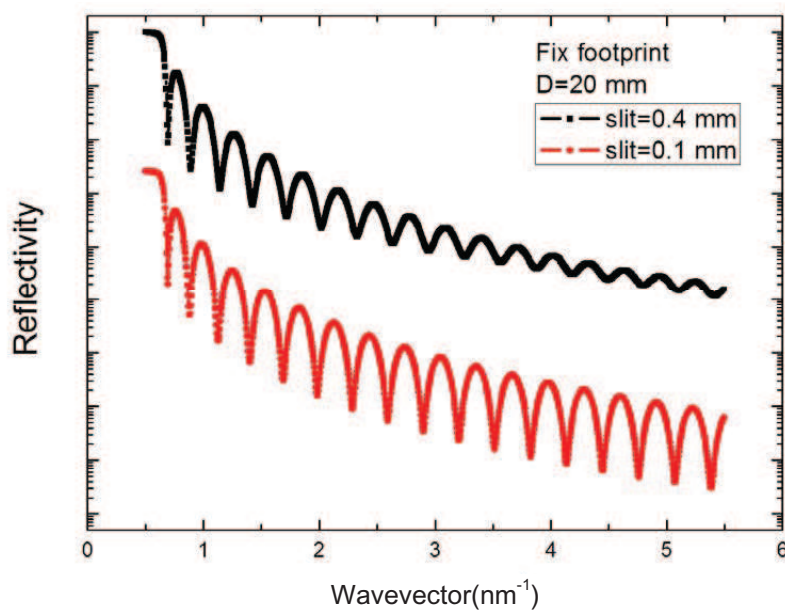


FIG. 4: The reflectivity curve calculated at the slit size of 0.4 mm and 0.1 mm at source to substrate distance of 20 mm. The X-ray footprints on the samples are fixed.

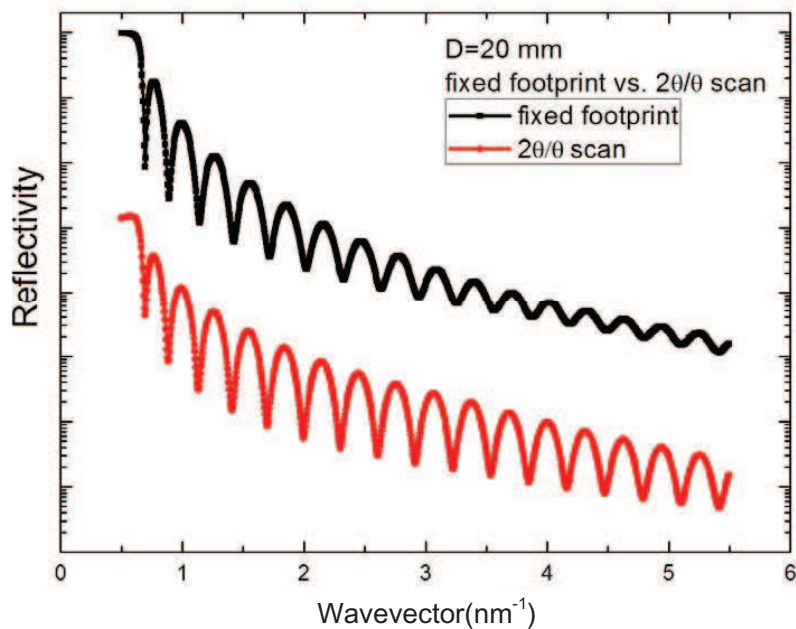


FIG. 5: A comparison of calculated reflectivity curves of the cases between  $2\theta/\theta$  scan and fixed footprint, at source to substrate distance of 20 mm.

Fig. 6 shows a simulation result of these two cases using  $2\theta/\theta$  scan. We assumed that the averaged thickness of the sample is 20 nm and the averaged surface roughness is 1 nm. Curve (a) shows the model of the lateral length scale within  $\xi_{\text{surface}}$ ; Curve (b) shows the result of lateral length beyond the  $\xi_{\text{surface}}$ . We used Eq. (4) to calculate the former case and Eq. (3) to calculate the later one. From Fig. 6, we can see the oscillation amplitude damped due to the surface roughness. For the case of lateral island size much larger than the  $\xi_{\text{surface}}$ , this damping is more rapid than the case of lateral island size smaller than the  $\xi_{\text{surface}}$ . The island grow model under fixed footprint scan or  $2\theta/\theta$  scan essentially have the same result if the surface morphology is similar across the whole sample.

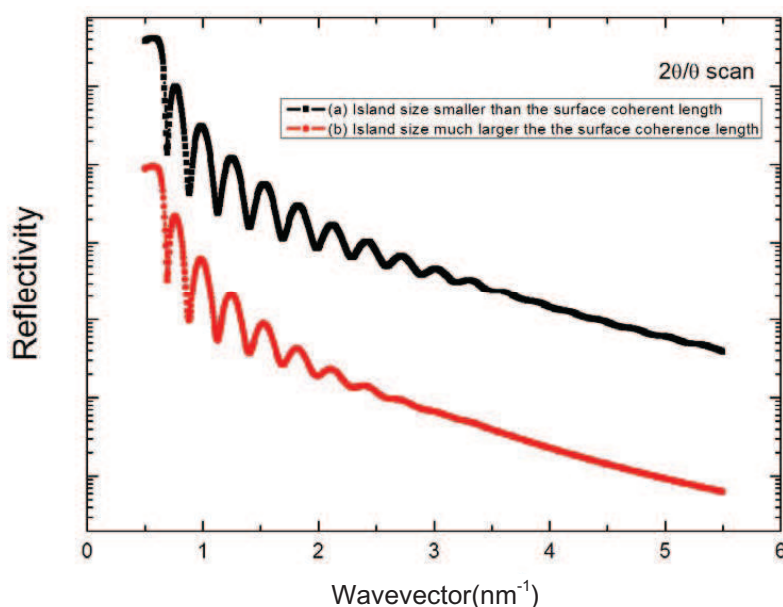


FIG. 6: A comparison of calculated reflectivity curves of  $2\theta/\theta$  scan for the 20 nm thin film with island growth mode. (a) the lateral island size smaller than the surface coherent length; (b) the lateral island size much larger the surface coherence length.

#### IV. CONCLUSION

In the specular reflectivity measurement, non-uniformity of the thin film could cause a drastically change in the reflectivity curves. For the case of non-uniform thin film during the deposition at a short source to substrate distance, reducing the footprint by narrowing down the incident slits, the thin film parameters can be determined in a better accuracy. Nevertheless, by narrowing down the slits means a loss of reflectivity intensity, which limits the maximum  $q$  range that can be probed. To guarantee the accuracy of determining the thin film parameters with a program based on the model of uniform thin film thickness, it

is better to keep the distance of evaporation source to the substrate to be 10 times longer than the sample size. For the case of island growth, the non-uniformity of the thin film is due to the grown island size being well beyond the surface coherent length of incidence beam. Narrowing down the silt is not sufficient to obtain well-resolved reflectivity data. In this case, the incidence beam coherent length should be enlarged to avoid this problem. When the lateral island size grows much larger than the surface coherent length of the incident beam, the reflected intensity from each island is superpositioned together without interference from the each island.

### Acknowledgements

This work was partly supported by the National Science Council under the project number of NSC99-2112-M007-018-MY3.

### References

- [1] X. L. Zhou and S. H. Chen, Phys. Rep. **257**, 223(1995).
- [2] S. Dietrich and A. Haase, Phys. Rep. **260**, 1(1995).
- [3] J. R. Lu, E. M. Lee, and R. K.Thomas, Acta Cryst. **A52**, 11(1996).
- [4] H. C. Su, C. W. Hu, J. J. Peir, *et al.*, Chin. J. Phys. (Taipei) **45**, 374 (2007).
- [5] H. C. Su, C. H. Lee, M. Z. Lin, *et al.*, Chin. J. Phys. (Taipei) **50**, 291 (2012).
- [6] C. H. Chou, Chin. J. Phys. (Taipei) **34**, 58 (1996).
- [7] L. G. Parratt, Phys. Rev. **95**, 359 (1954).
- [8] A. van der Lee, F. Salah, and B. Harzallah, J. Appl. Cryst. **40**, 820 (2007).
- [9] C. H. Lee, F. G. Guo, and C. C. Chu, Chin. J. Phys. (Taipei) **50**, 311 (2012).
- [10] C. H. Lee, K. L. Yu, and H. C. Lee, Nucl. Instr. Meth. A **467–468**, 1073 (2001).
- [11] V. Rossi Albertini, B. Paci, and A. Generosi, J. Phys. D: Appl. Phys. **39**, R461 (2006).
- [12] C. H. Lee, and S. Y. Tseng, J. Appl. Cryst. **31**, 181 (1998).
- [13] C. H. Lee, H. Y. Lee, K. S. Liang, *et al.*, Physica B **248**, 109 (1998).
- [14] D. Windover, E. Barnat, J. Summers, *et al.*, J. Electron Mater. **31**, 848 (2002).
- [15] T. Salditt, H. Rhan, T. H. Metzger, *et al.*, Z. Phys. B **96**, 227 (1994).